Patterns in Isotopic Compositions and Magic Numbers: Insights from a Geometric Model

Jingfeng Lin*

South China University of Technology, Guangzhou, 510641, China
*Email: aulin@mail.scut.edu.cn

Abstract. This paper identifies a regularity in the composition of isotopes and the magic number phenomenon, where nuclei exhibit enhanced stability when the number of nucleons, A, approaches or equals S(S+1) - 2. Using S as the shell number, we derive a nucleon arrangement model consistent with magic numbers and the evolution of shell structure. These patterns emerge from an intriguing torus-helix model with three lobes, resembling Kelvin and Maxwell's concept of vortex structures, and align with Rutherford's neutron hypothesis. Furthermore, the proposed toroidal helix nucleon cloud model, which possesses a string-like structure, aligns with the concept of "interactions between strings" insightfully observed in resonance states and Veneziano four-point amplitudes in String Theory.
Keyword. Shell model; isotopic compositions; magic numbers; nucleon arrangement; vortex knot; string theory.

1. Introduction

The nuclear shell structure, characterized by magic numbers, is a fundamental concept in nuclear physics [1–7]. Despite its significance, the microscopic origins of this structure are still actively debated. Circular and elliptical motions are two-dimensional and insufficient to describe the three-dimensional nature of atoms, such as the external single electron of hydrogen atoms [8] and the three quarks within a single proton [9]. This prompted us to explore diverse motion patterns capable of forming a spherical shape. Among various three-dimensional configurations, our attention was captivated by a three-lobed structure resembling a DNA-like double helix connected at both ends, bent into a ring-shaped standing wave. This trefoil knot vortex structure, extendable from a torus to a sphere, possesses an intrinsic spin of two loops (see figure 6) and resembles fundamental atomic components. Microscopic vortices and knots have been widely studied [10–16]. Comparing this structural unit with the characteristics of neutrons and protons, we gradually made several discoveries, including the correlation of combined results from multiple units with isotopic compositions and magic numbers.

This exploration has led to the identification of a closely packed nucleon arrangement pattern. According to this arrangement pattern, we initially observed that nucleons in ^{208}Pb could form a complete pattern, with the nucleon number A = 14(14+1)-2. Subsequently, we found that 37.2% of naturally occurring even-Z isotopes with the highest relative abundance were associated with the relation A = S(S+1), where S denotes the total number of shells. This relationship correlates with the inversion of elemental atomic weights. From this, we inferred that nucleons in ^{208}Pb closely aggregate to fill S2 to S14 shells in a specific spatial pattern, and we extrapolated similar arrangements for other magic nuclei. Guided by this preliminary configuration, we deduced rules governing nucleon arrangements based on unique combinations of neutron and proton numbers in various isotopes, where

neutron or proton totals align with certain closed-shell configurations, a topic explored in Section 4. The torus helix "nucleon cloud" model is introduced in Section 5.

Preliminary analysis suggests that the clustered patterns of nucleons in our model align with collective resonance phenomena. The three-dimensional torus shell distribution patterns of nucleons suggest its association with the neutron skins and halos phenomenon. Furthermore, our proposed torus helix nucleon model must possess string-like properties due to its pattern of interaction and close packing, which has interesting connections with string theory and has prompted further exploration. The origin of string theory lies in the Veneziano four-point amplitude, which may describe the vibrational modes of strings and their interactions (scattering amplitudes) with hadrons [17–22].

2. Nucleon Count A=S(S+1)-2 in Isotopic Compositions

The isotopic composition of elements [23] provides a quantifiable foundation for delving into concealed intricate microstructures. We conducted a comprehensive investigation into the nucleon numbers of naturally occurring isotopes across all 43 even-Z elements. Within this exploration, a remarkable revelation surfaced – nine elements exhibited their most abundant isotope with nucleon numbers conforming to the relation:

$$A=S(S+1)-2, \tag{1}$$

where A represents the nucleon number, and S takes on positive integer values. Among these nine nuclides, four were doubly magic nuclei, including ${}_{2}He_{2}$, ${}_{20}Ca_{20}$, ${}_{82}Pb_{126}$ and ${}_{14}Si_{14}$. The roster also included the magic nucleus ${}^{88}Sr_{50}$ with a neutron number of 50 and the heaviest known stable nuclide, ${}^{238}U$. Furthermore, five nuclides with the highest relative abundance aligned with A = S(S+1). These nuclides were ${}^{12}C$, ${}^{20}N$, ${}^{56}Fe$, ${}^{132}Xe$, and the magic nucleus ${}^{90}Zr_{50}$. Figure 1(a) presents a bar chart illustrating the relative abundance of naturally occurring even-Z isotopes.

Preliminary results indicate that approximately one-third of even-Z elements reveal a continuous shell pattern, as shown in the top row of figure 1(a), with S values ranging from 2 to 15. A preliminary matching of S shell levels can be made based on the neutron and proton numbers of each nuclide. Figure 1(b) categorizes the most abundant isotope of each element into respective shell levels, displayed in vertical columns, while showing the difference between the nucleon number of the isotope and S(S+1) in horizontal rows. Each magic nucleus corresponds to a specific S shell level based on the associated magic number. This graph clearly highlights the notable alignment of nucleon numbers within the heavy nuclear region. Specifically, nuclides such as ${}^{180}Hf$, ${}^{208}Pb$, ${}^{238}U$, and ${}^{270}Hs$ adhere to the relation (1), corresponding to shell levels 13, 14, 15, and 16. The inclusion of A=270 is substantiated by data sourced from the NuDat database, where the Delta Alpha Q-value plot indicates that the proton number 108 and neutron number 162 exhibit characteristics indicative of magic numbers. Furthermore, the three even shell levels, S8, S10, and S12, do not align with any magic numbers. A potential explanation for this observation lies in the stability conferred by odd closed neutron-shell configurations. Specifically, for the proton numbers associated with these three shells, neutron numbers tend to adhere to a stable ratio range, and when these neutrons self-organize into odd closed shells, they exhibit greater stability than in even shell configurations. Specific nucleon arrangement patterns, such as those corresponding to magic numbers, will be discussed in Section 4.

In conclusion, this hierarchical ordering of stable isotopes suggests the presence of a pattern resembling fully occupied shell levels in nucleon arrangement.

3. Nucleon Count A=S(S+1)-2 in the Inversion of Elemental Atomic Weights

It's worth noting that among the stable isotopes listed in figure 1(b) that adhere to the relation (1), ${}^{40}Ar$, ${}^{130}Te$, and ${}^{238}U$ are linked to a phenomenon known as the inversion of elemental atomic weights. These isotopes possess more neutrons than the subsequent element in the atomic sequence (corresponding isotopes [23] being ${}^{39}K$, ${}^{127}I$, and ${}^{237}Np$, respectively), resulting in a heavier atomic weight. Moreover, the isotope ${}_{28}Ni_{30}$ notably exhibit fewer neutrons, while ${}^{208}Pb$ have more neutrons. Additionally, among the isotopes of tellurium, ${}^{126}Te$ is the most stable, whereas the most abundant isotope, ${}^{130}Te$,

exhibits both a lower average binding energy and undergoes 2β- decay due to an excessive number of neutrons. Similarly, within the isotopes of the element iron, ^{58}Fe exhibits the highest average binding energy, while ^{56}Fe exhibits the highest relative abundance. In contrast, ^{54}Fe with Neutron Magic Number 28, has a lower abundance. All these phenomena are closely associated with the relation (1).

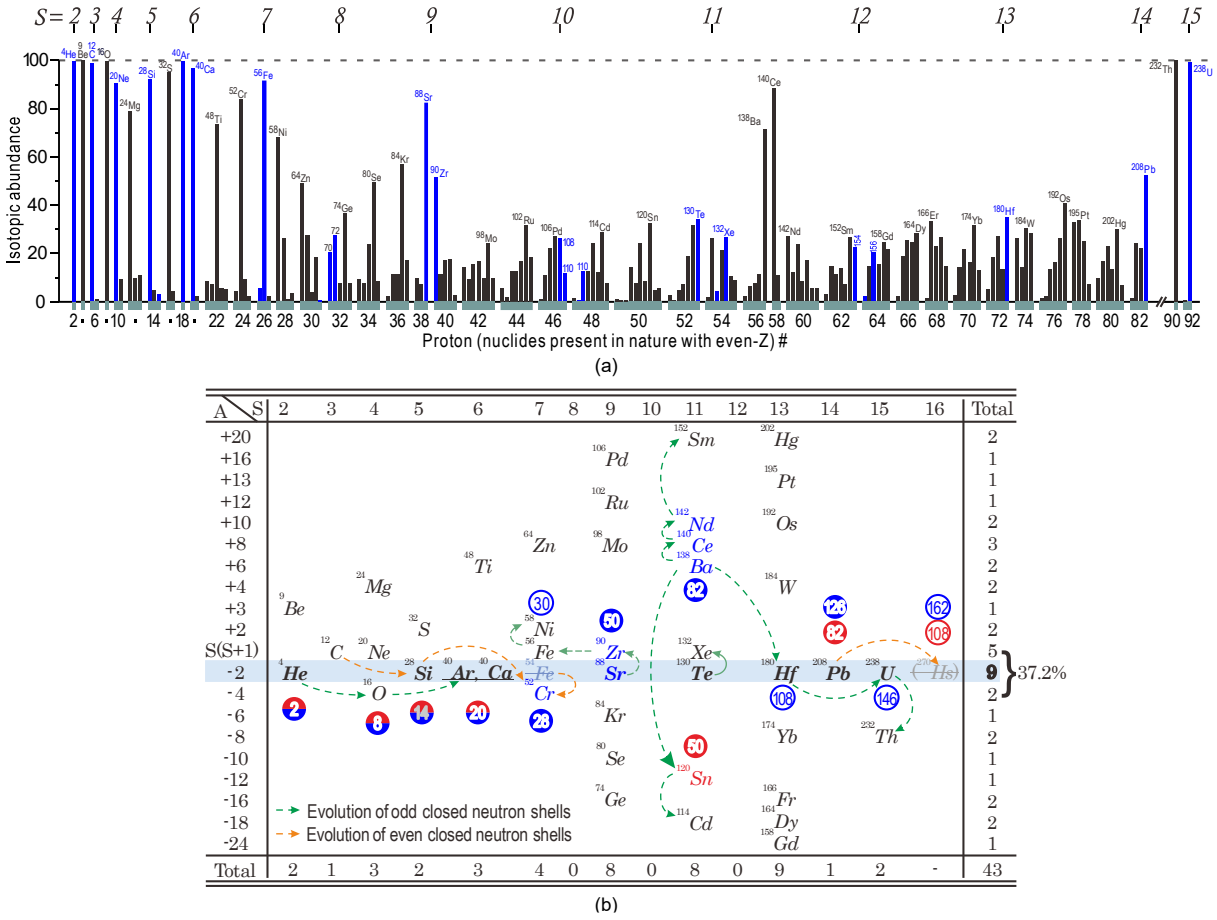

(a) The bar graph illustrates the relative abundance of even-Z isotopes. The natural element sequence reveals 15 consecutive levels. **(b)** Vertical columns represent the S levels corresponding to even-Z isotopes with the highest relative abundance, based on the relation A = S(S+1) - 2 and certain nucleon arrangement rules. Horizontal rows display the relationship between nucleon number and A = S(S+1) for each isotope. The figure indicates that 37.2% of isotopes are relatively concentrated around A = S(S+1) - 2. Data sourced from NIST [23].

Figure 1. Pattern of even-Z isotopes with the highest relative abundance.

4. Arrangement Patterns Corresponding to Magic Number Phenomena

This section introduces a nucleon arrangement model that aligns with the potential indication of relation (1). Within this model, we have derived specific schemes for the spatial distribution of nucleons corresponding to magic numbers. Figures 2 and 3 illustrate the nucleon distribution patterns in a cutaway view, originating from a three-dimensional helical closed-string nucleon cloud structure. Our analysis draws parallels to the extranuclear electron cloud, conceptualizing individual nucleons as orbital clouds. This framework provides a foundation for studying how nucleon clouds interact, particularly the electromagnetic interactions among nucleons.

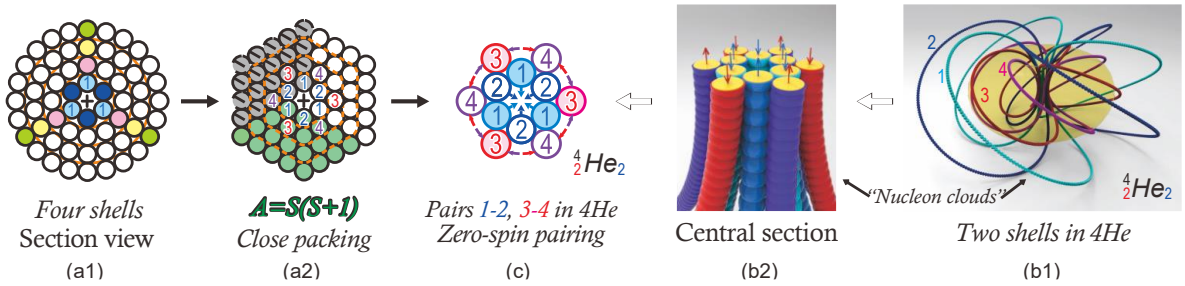

(a1, a2) Each nucleon consists of three rotationally symmetric units, closely packed to form a hexagonal pattern. Green circles arranged in a parallelogram indicate full shell occupation, achieving the total nucleon count A = S(S+1). **(c)** According to pairing effects [2, 9, 24–27], two anti-parallel protons exhibit a uniform arrangement in the S2 shell (self-organization), while two anti-parallel neutrons occupy the S1 shell. In this scenario, four nucleons couple to a state characterized by angular momentum zero, forming ^{4}He *with* spin-zero. **(b2)** Center cross-section diagram based on the three-dimensional structure model of ^{4}He. **(b1)** Perspective view of the three-dimensional model of ^{4}He: Two protons (3 and 4) exhibit a uniform distribution in the S2-torus shell, while two neutrons (1 and 2) exhibit a uniform distribution in the S1-torus shell. The analysis draws parallels to the extranuclear electron cloud, conceptualizing individual nucleons as orbital clouds.

Figure 2. Principle of arrangement model.

As is well known, the Standard Model of particle physics describes nucleons as composed of three quarks [28]. SLAC deep inelastic scattering experiments [29, 30] have revealed that the constituents of a proton exhibit a 1/3 baryon number [31]. Consequently, we postulate that each nucleon comprises three geometric units that exhibit rotational symmetry. Given the similar behavior and comparable masses of protons and neutrons, implying analogous structures and shapes, we further assume that the three geometric units of neutrons and protons have the same circular cross-sections. Subsequently, we present a nucleon arrangement principle demonstrated in figure 2, where nucleons are densely packed with nucleon numbers A = S(S+1) when all the shells are filled. According to the phenomenon of zero-spin and magic numbers, we deduce optimal arrangement schemes for Magic Numbers 2, 8, 14, 20, 28, 50, 82, and 126. Figure 3 illustrates the arrangement schemes for these magic numbers, highlighting their common structural characteristics.

Neutron Magic Number 2 corresponds to a filled neutron shell in S1, forming a closed shell, as shown in figure 3(a1); Magic Number 8 corresponds to a filled neutron shell in S3, forming a closed shell, as depicted in figure 3(b); Magic Number 20 involves expanding the shell to S5 based on Magic Number 8 to form two closed shells, as presented in figure 3(c); Neutron Magic Number 50 corresponds to instances where shells S9 and S7 are filled with neutrons, forming two closed shells, as shown in figure 3(d). Proton Magic Number 50 corresponds to six odd-numbered shells filled with neutrons, as presented in figure 3(e). In this case, the neutron number is Magic Number 82. Based on the nucleon number of ^{208}Pb, Proton Magic Number 82 corresponds to seven even-numbered shells filled with neutrons, as depicted in figure 3(h). In this scheme, the neutron number is Magic Number 126. Significantly, as 126 neutrons and 82 protons reach a filled arrangement, each neutron is adjacent to at least one proton, resulting in a structure maintaining impeccable sixfold symmetry. Neutron Magic Number 28 corresponds to instances where even-numbered shells S6, S4, and S2 are filled with neutrons, as shown in figure 3(g); and Magic Number 14 [32] corresponds to instances where even-numbered shells S4 and S2 are filled with neutrons, as depicted in figure 3(f). In all instances in figure 3, the arrangement of neutrons distinctly showcases the importance of maximizing closed neutron shells. Moreover, each neutron being directly adjacent to at least one proton highlights the significance of proton-neutron coupling.

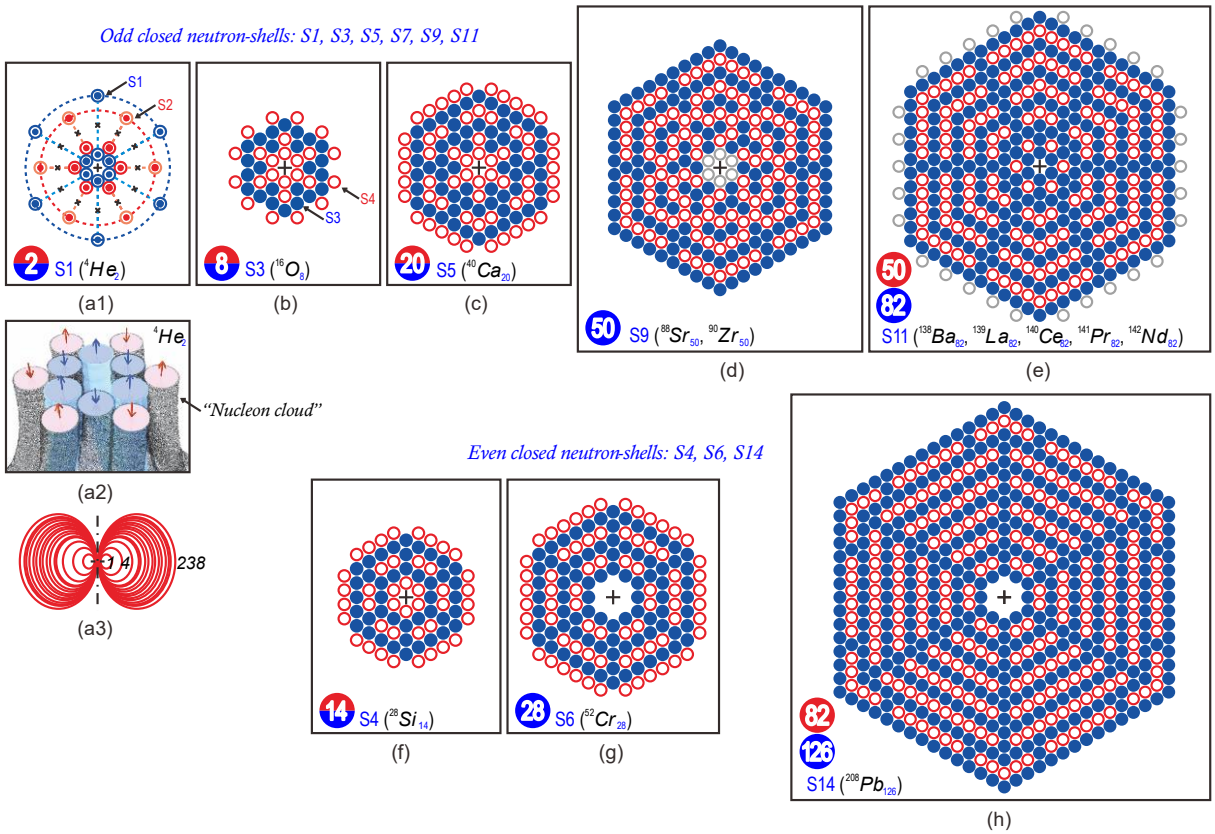

Blues represent neutrons, and reds represent protons. **(a1)** Sectional diagram illustrating an arrangement mode for ^{4}He with Magic Number 2. The cross (x) symbol indicates an inward direction into the paper, and the point symbol indicates an outward direction. **(a2)** Center cross-section diagram based on a three-dimensional orbital cloud model of ^{4}He. **(a3)** Side view of shell distribution. **(b)** ^{16}O with Magic Number 8. Two adjacent protons must be aligned antiparallel to each other. **(c)** ^{40}Ca with Magic Number 20 [32], derived by adding shells from ^{16}O. **(d)** Magic Number N = 50, and N = 30 [33]. **(e)** Magic Number Z = 50 and N = 82, complete six odd-numbered closed neutron shells. **(f)** ^{28}Si with Magic Number 14 [34], two even-numbered closed neutron shells; ^{22}O with Magic Number 14 [34]. **(g)** ^{52}Cr with Magic Number N = 28, three even-numbered closed neutron shells, derived by adding shells from ^{28}Si; ^{42}Si [32, 35] with N = 28, Z = 14. **(h)** Magic Number Z = 82 and N = 126. Nucleons filled the S2 to S14 shells, and all nucleons participated in N-P pairing [36], considering maximal symmetry and the neutron skin phenomenon of ^{208}Pb.

Figure 3. Schematic of arrangement corresponding to magic numbers.

The above-mentioned arrangement model incorporates several essential rules and principles. It is crucial to identify commonalities among all nuclides while ensuring that any rules align with the inherent properties of atomic nuclei and nucleons. Below is a further discussion on the arrangement model:

1. Pairing Resulting in Zero Spin [37]: Pairing effects in even-even nuclei result in a total angular momentum of zero. Typically, protons (or neutrons) pair up in twos, exhibiting rotational symmetry and antiparallel arrangement, as depicted in figure 2(b2). This rule adheres to the Pauli exclusion principle.

2. Maximizing Neutron-proton Coupling: Neutron-proton interactions are crucial for binding the nucleus maximally, and nucleon arrangements need to maximize N-P coupling [38]. As shown in figure 3, N-P pairing occurs between adjacent neutrons and protons. This relates to the charge independence of nuclear forces, which do not distinguish between protons and neutrons. Guided by pairing correlations and the Pauli exclusion principle, experimental data of average binding energies suggest that both parallel and antiparallel proton-neutron combinations contribute to the binding

energy. This contribution is evident in the binding energy data for ${}_1H_1$(1112 keV), ${}_1H_2$(2827 keV), and ${}_2He_1$ (2573 keV) states, for instance. Data sourced from NuDat. Also refer to [27].

3. Filling each shell sequentially: This aligns with the nucleon number pattern, directing cohesion within the nucleus toward the central high-density region.

4. Symmetry: The stability of atomic nuclei is positively correlated with the symmetry of nucleon arrangements.

5. Neutrons segregating or surrounding protons.

6. Formation of closed neutron shells: This is a factor in the magic number phenomenon. Experimental evidence suggests a quasi-bound resonance-like feature between neutrons [39].

7. Proton Pairing: Even in a two-dimensional arrangement, protons are difficult to separate individually by a limited number of neutrons. This suggests that a tightly bound nucleus should have adjacent protons. As depicted in figure 3, two adjacent protons must be oriented in opposite directions, aligned antiparallel to each other, and there are no more than 11 consecutive adjacent protons. This gives rise to a novel concept, suggesting that electromagnetic attraction might occur between protons with a parallel arrangement, contributing to the counteraction of strong Coulomb repulsion.

8. Simple Patterns [40–46]: *Many nuclei exhibit remarkably simple regularities* [40]. The configuration pattern depicted in figure 3 follows clear rules of simplicity. For instance, the number of nucleons that a single shell can accommodate increases by increments of +2. The S1 shell accommodates two nucleons, the S2 shell accommodates four, and so forth.

The two-dimensional nucleon arrangement model presented in this section aligns with various manifestations of nucleons. However, the physical world operates in three-dimensional space. In the subsequent section, we will introduce a fundamental overview of the three-dimensional model framework for nuclear structure, essential for capturing a wider range of nuclear properties.

5. A Preliminary Overview to the Fundamental Three-Dimensional Structural Model

In experimental observations, nuclei near closed shells exhibit a spherical shape, indicating a state of spherical equilibrium. *Atomic nuclei exhibit a well-defined size and edge, while protons, as revealed by electron-proton scattering, lack a well-defined edge*. Circular and elliptical motions are two-dimensional and insufficient to describe the three-dimensional nature of atoms, such as the external single electron of hydrogen atoms and the three quarks within a single proton. This prompted us to explore diverse motion patterns capable of forming a spherical shape. Among various three-dimensional configurations, our attention was captivated by a three-lobed structure resembling a DNA-like double helix connected at both ends, bent into a ring-shaped standing wave. This structure, extendable from a torus to a sphere, possesses an intrinsic rotational period of two loops, equivalent to 720 degrees. Comparing this structural unit with the characteristics of neutrons and protons, we gradually made several discoveries, including the correlation of combined results from multiple units with isotopic compositions and magic numbers.

We transformed the double helix with a wave number of 1.5 into a toroidal structure with standing wave characteristics, as depicted in figure 4. Figure 4(a1) illustrates a three-dimensional representation of a model unit created by bending the double helix with a wave number of 1.5 into a smoothly connected torus-helix structure. The top view in figure 4(a2) highlights its tri-symmetric feature. Figure 4(b1) demonstrates the uniform distribution of two model units on a torus, with the central regions of these units in close proximity. Furthermore, figure 4(b2) presents a cross-sectional structure at the region of highest density in the central area. This structure corresponds entirely to the two-dimensional model detailed in the preceding section, offering the complete three-dimensional shape of the two-dimensional model. Figure 4(c) presents a perspective view of the four nucleon clouds within ${}^4He$.

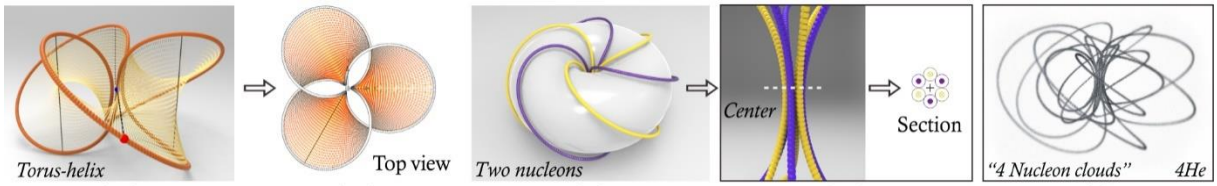

(a1) Schematic representation of a toroidal structure formed by bending a double helix with a wave number of 1.5. **(a2)** Top view of the three-dimensional model. **(b1)** Two helix units evenly distributed on a torus. **(b2)** Cross-sectional structure at the core of highest density in the central area. **(c)** Perspective view: 4 nucleon clouds within ^{4}He.

Figure 4. A fundamental contour for nucleon.

We refer to the model depicted in figure 4(a1) as a "torus helix unit," characterized by its fundamental attributes of exhibiting triple rotational symmetry and a smooth curvature along a torus. When multiple torus helix units closely intertwine as shown in figure 4(c), all unit centroids overlap, and they organize into concentric shells while maintaining individual spatial independence. An idea emerging from this model is the overlap and arrangement of all nucleons within the nucleus into concentric shells, making it visually impossible to distinguish individual nucleons in the appearance of the atomic nucleus.

For this distinctive and unconventional form, we aim to strengthen the alignment between our model and experimental findings or physical phenomena. For instance, a study exploring toroidal configurations experimentally observed numerous excited states of ^{12}C decaying primarily into three alpha particles. Notably, the triangular clustering of these alpha particles exhibits significant overlap with a torus [47-48]. Below, we present preliminary insights into the potential utility of this model in elucidating certain nuclear characteristics.

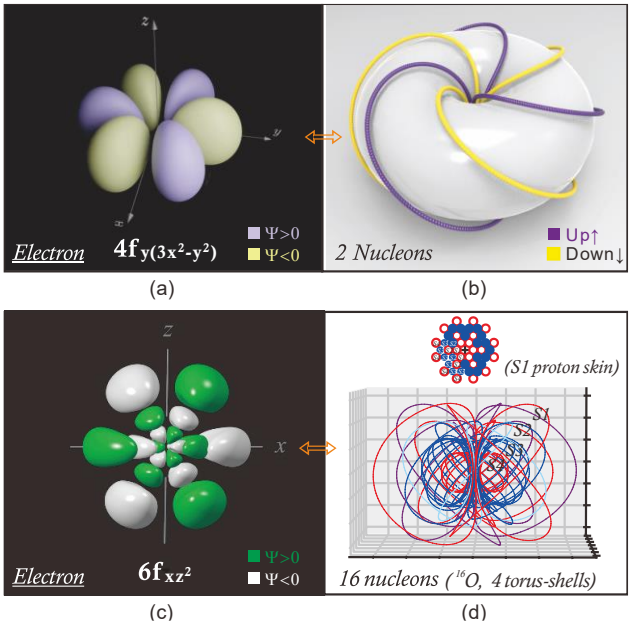

(a) The 4f.y($3x^2$-y^2) orbital, see Ref. [49].
(b) Two torus-helix units.
(c) The 6f.xz^2 orbital, see Ref. [49].
(d) Multiple torus helix units. Here, a novel concept suggests that electromagnetic attraction might occur between protons with a parallel arrangement, contributing to the counteraction of the strong Coulomb repulsion. Similarly, there is also electromagnetic attraction when the direction of opposite charges is antiparallel.

Figure 5. Comparing the shape of the torus helix model to the probability density iso-surfaces of hydrogen atomic electron orbitals.

1. Describing the Shapes of Nucleons: Our analysis draws parallels to the extranuclear electron cloud, conceptualizing individual nucleons as orbital clouds. As probability distributions derived from wave functions form the foundation of our understanding, comparing the imagery of the torus helix model to probability density distribution images of extranuclear electrons obtained by solving the

Schrödinger equation, as shown in figure 5, it is evident that the torus helix model fundamentally aligns with the principles of the Schrödinger equation. The left and right images in figure 5 both define various quantum states, including radial quantum numbers, angular momentum quantum numbers, and magnetic quantum numbers, and can be transformed into a toroidal shape. The transition between the torus helix and the sphere helix is shown in figure 5. Both the torus helix units and the sphere helix units exhibit the characteristics of standing waves.

2. Microscopic Theories: Figures 4, 5(b), 5(d), and 6 illustrate the vortex model, which builds upon microscopic theories studied by scientists such as Maxwell and Kelvin [10–16]. Maxwell spent a considerable amount of time studying molecular vortex theory [10, 11], and Kelvin proposed that atoms (then considered as fundamental particles) could be described as knotted vortex rings [12, 13].

3. Neutron Skin and Neutron Halo: The outermost shell of the nuclear model is evidently S1, followed by S2. When the outermost shells are all occupied by neutrons, a neutron skin or neutron halo forms. The model image in figure 5(d) illustrates four torus helix units within the S2 shell. During α decay in heavy nuclei, four nucleons are emitted. According to the arrangement model, it can be inferred that all four nucleons in the outermost S2 shell are more likely to collectively depart from the parent nucleus.

4. Triple Rotational Symmetry: As depicted in figure 4(a2), this triply symmetric shape resembles a Möbius strip, featuring three 180-degree torsions, resulting in a spin period of 720 degrees.

5. Precession: The torus helix units are formed by dual helices surrounding a central point, similar to a spinning top. Neutrons are electrically neutral particles with a non-zero intrinsic spin, which makes them sensitive to magnetic fields. When a neutron is placed in a magnetic field, its spin precession occurs around the direction of the field, leading to a phase shift that can be experimentally observed [50, 51].

6. Short-Range Nature of Nuclear Forces: As seen in figure 5(d), the denser central region corresponds to enhanced nuclear forces, unequivocally demonstrating the short-range nature of nuclear forces.

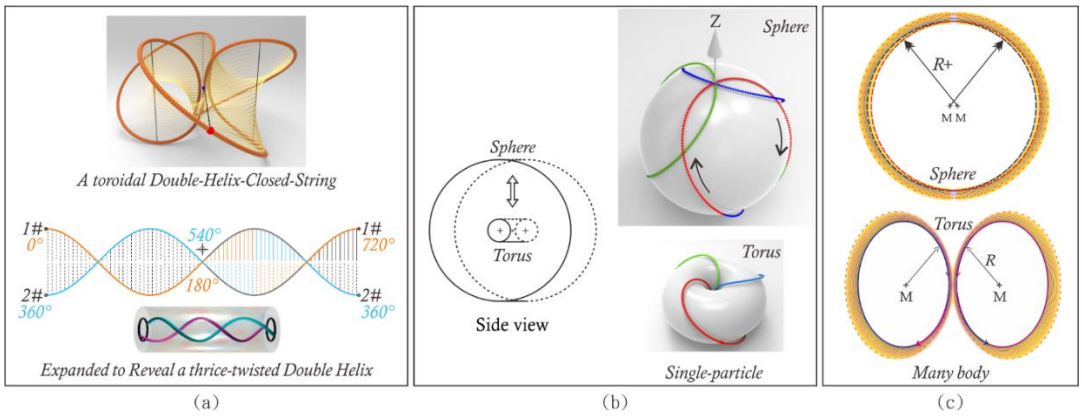

(a) A thrice-twisted double-helix-closed-String and expanded to reveal a thrice-twisted double helix. Bottom pic is taken from [16]. **(b)** Increasing the diameter of the helix transforms the toroidal shape into a spherical form while preserving the double helix feature within. **(c)** Schematic representation of the transition from a multi-shell torus helix to a multi-shell sphere helix.

Figure 6. Transition between torus helix and sphere helix.

7. Collective Resonances: As depicted in figure 5(d), all nucleons closely couple in the central region, a structural configuration in accordance with the characteristics of nucleonic collective resonance.

8. Transformation into Sphere Helix: The torus helix can be transformed into a sphere helix, as illustrated in figure 6. Figure 6(b) presents a three-dimensional model, demonstrating that the double

helical property is retained within a spherical configuration. Figure 6(c) depicts the transition from a multi-shell toroidal structure to a multi-shell spherical structure.

9. Helix Structure and Symmetry: The helix structure can be either right-handed or left-handed, and this property remains invariant regardless of the reference frame. Flipping the torus helix by 180 degrees keeps its shape unchanged.

10. Electromagnetic Interactions: Nucleons carry positive or negative charges, thus exhibiting attractive or repulsive interactions. The vortex helix nucleon model must possess string-brane properties due to its pattern of interaction and close packing. String theory [17–22] may further validate this model. A schematic representation of the hypothesized nucleon-nucleon interaction mechanism is shown in figure 8.

11. Electromagnetic Resonance Phenomena [52, 53]: Figure 9 shows the electromagnetic oscillation phenomena observed in the BESIII experiment [53]. The nearly orthogonal oscillations are attributed to the influence of resonant structures. We hypothesize, with cautious optimism, that the vortex helix nucleon model exhibits potential validity for electromagnetic resonance.

6. Correspondence with Magnetic Moments and Spin

Our model necessitates an accurate depiction of the nucleon arrangement patterns for all nuclides in their ground states. Upon examining the nucleon arrangement schemes for a broader range of nuclides based on specific neutron and proton numbers, it is observed that individual unpaired neutrons or protons, in certain instances, can only be arranged in the lowest S1 shell, while deviations in neutron or proton numbers result in them being arranged only in the highest shell. This pattern aligns with achieving the highest symmetry state when adhering to general rules. This observation is consistent with the magnetic moments and spins of the corresponding nuclides, as detailed in figure 7. The distribution of levels is similar to that of mainstream nuclear shell models. Concrete conclusions require further comprehensive and in-depth investigations. Based on experimental effects such as magnetic moments, spins, parity, and nuclear halos (skins), further comparisons can be made with various nuclear structure models. Our model agrees with the principles of the Gamow shell model [54], which efficiently describes weakly bound nuclear systems by considering both internucleon correlations and continuum coupling.

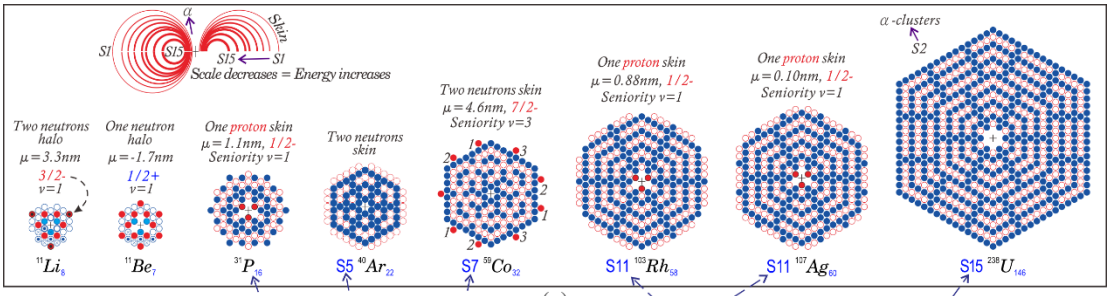

Neutron Shell	1	2	3	4	5	6	7	8	9	10	11	12	13	14	15	16
Magic Number	2		8	14	20	28	30		50		82 50		108	126 92	146	162 108
Isotopes	^{4}He		^{16}O ^{20}Ne ^{24}Ne ^{31}P ^{31}S	^{28}Si ^{22}O ^{27}Al ^{32}S	^{40}Ar ^{40}Ca ^{48}Ti	^{42}Si	^{56}Fe ^{55}Mn ^{58}Ni ^{59}Co ^{64}Zn ^{74}Ge ^{68}Ni		^{81}Kr ^{98}Mo ^{101}Rh ^{115}In ^{103}Rh ^{105}Ag ^{88}Sr ^{107}Ag ^{90}Zr ^{109}Ag		^{120}Sn ^{138}Ba ^{130}Te ^{139}La ^{132}Xe ^{140}Ce ^{132}Sn ^{141}Pr ^{159}Tb ^{142}Nd		^{164}Dy ^{184}W ^{160}Fr ^{192}Os ^{174}Yb ^{195}Pt ^{180}Hf ^{188}Hg ^{232}Th ^{235}U	^{208}Pb ^{209}Bi ^{209}Po ^{210}Po ^{212}Rn	^{238}U ^{241}Am ^{242}Cm	^{270}Hs

(b)

(a) Proposing the two-neutron halo structure in ^{11}Li and the single-neutron halo in ^{11}Be. The low-energy magnetic moment in ^{31}P indicating one proton skin in the S1 shell. Predicting a stable two-neutron skin in ^{40}Ar. Schematic representation of three unpaired protons in ^{59}Co with a seniority number of 3. Unpaired protons occupying the S1 shell for ^{103}Rh and ^{107}Ag (see Ref. [55]). Magnetic moment data are obtained from Ref. [56]. **(b)** A preliminary attempt to correlate all nuclides with their respective shell levels and magic numbers.

Figure 7. Nucleon arrangements and nuclear characteristics for selected nuclei.

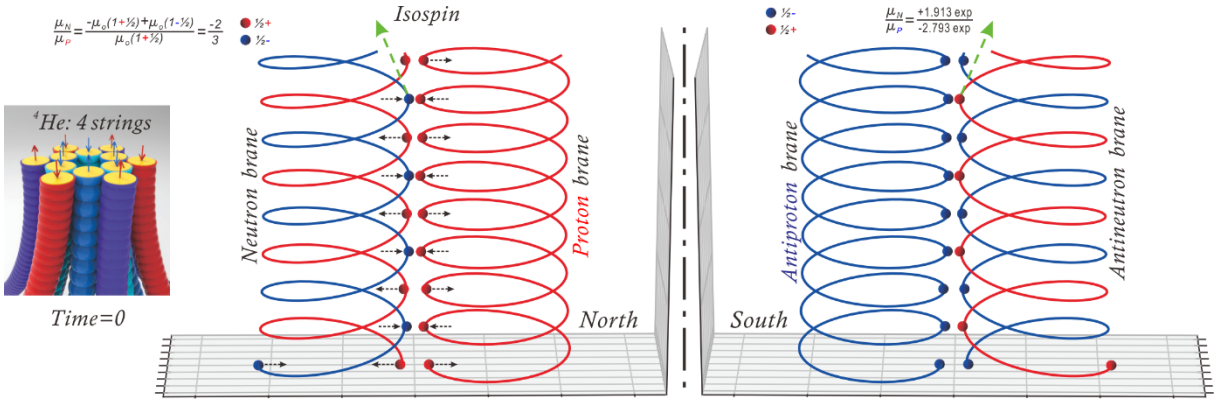

The vortex helix nucleon model exhibits string-like and brane-like properties, where nucleons, carrying positive or negative charges, interact through attraction or repulsion. The illustrations provided here represent abstract eigenstates and must theoretically consider quantum effects (quantum states). In our universe, electrons predominantly spin to the left [57]. Feynman noted, "*In fact, it was checked right here at Caltech by Boehm and Wapstra, that the electrons spin mostly to the left. (There were some other experiments that gave the opposite answer, but they were wrong.)*" For instance, electrons released by the decay of ^{60}Co exhibit left-handed spin [58]. It can be inferred further that nucleons in matter are right-handed, while those in antimatter are left-handed [57]. Furthermore, this can be linked to Rutherford's neutron hypothesis [42], where Rutherford posited, "*We also have strong reason for believing that the nuclei of atoms contain electrons as well as positively charged bodies; the electron forms a very close and powerful combination with the positively charged units.*" Additionally, Wheeler suggested that perhaps the universe in its totality is made only of electrons, positrons, and photons [59]. All charged particles participate in a collective resonance that confines them within the "nuclear potential well". In other words, electrons behave as quarks and engage in strong interactions, being closely coupled within neutrons, thereby resolving the Klein paradox [60]. This speculation raises the possibility that quarks, which may carry fractional charges, could represent different "resonant states [61]" (fundamental particle resonances) in different environments. Two teams have observed that electrons can behave as if they had fractional charges (such as -2/3) and do so without being nudged by an external magnetic field [62, 63].

Figure 8. Hypothetical model for nucleon-nucleon interaction mechanism.

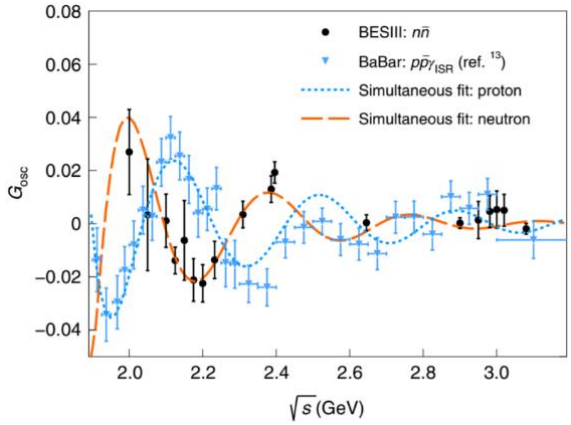

The BESIII experiment demonstrates that the effective form factor of neutrons exhibits periodic behavior, akin to observations of the proton's form factor. It is conjectured that the nearly orthogonal oscillations may result from the influence of resonance structures [53]. Neutrons exhibit electric neutrality but internally contain both positive and negative charges, while protons carry a charge of 1e+. Therefore, we infer that the model proposed in this paper can be correlated with the electromagnetic oscillations of neutrons and protons.

Figure 9. Nucleon form factor |G| following the dipole law [53].

7. Summary and Discussion

Our model proposes a three-dimensional configuration for atomic nuclei and nucleons, revealing a dense interaction pattern resembling two-dimensional arrangements at the core section. The nucleon arrangement aligns with experimental phenomena such as magic numbers, isotopic compositions, collective resonances, magnetic moments, and halo structures. We further postulate that quantum mechanical and relativistic effects are confined within the nucleon and electron clouds. The interaction mechanisms between nucleon clouds are analogous to those between electron clouds. Inside the atom, protons couple with extranuclear electrons and govern the fundamental patterns of their motion, while free electrons escape the constraints of the atomic nucleus.

Delving deeper into this model reveals inherent complexities. Here, we summarize pertinent discussions:

1. The shell model incorporates single-particle motion, where each nucleon possesses independent spatial motion. The radial distribution of energy level density in nuclear shell structures is intricately linked to the spatial distribution of nucleons. The arrangement of nucleons in spatial structures may align with the micro-origin of energy level distributions described by quantum mechanical probability densities [8]. The interaction mechanisms among nucleons remain uniform, whether in the ground state of light nuclei or the ground state of heavy nuclei. Our proposed three-dimensional model suggests a plausible scenario: in the high-density region of the core, local nucleon clouds exhibit collective close coupling, while the nucleon density decreases in the outer regions, as illustrated in figure 3(a3).

2. Our model suggests the necessity of subshells [3] in nucleon arrangements. ^{236}U contains clusters corresponding to 82N + 50P, facilitating the production of a *Ba* nuclide. After absorbing a neutron, ^{235}U undergoes asymmetric fission, producing a *Ba*. The double-humped fission yield curve for ^{235}U is almost exactly delimited. The asymmetry term is truly asymmetric [3]. The majority of fission events result in a division where one fragment has not fewer than 82 neutrons, and the other not fewer than 50 [1]. Considering that the nucleon arrangements of heavy nuclei contain clusters corresponding to magic numbers, we can attempt to correlate fission asymmetry with magic number phenomena.

3. Our research asserts that interaction mechanisms among nucleons must be consistent, whether in light or heavy nuclei. The fundamental laws governing nucleon arrangements are universally applicable. A study suggests that ^{42}Si is nearly spherical shape [35]. Our research unifies nucleon arrangement rules for both ^{28}Si and ^{42}Si.

4. Our model must account for deformation and shape coexistence within the nucleus. It is preliminarily believed that due to different positions or combinations, the interaction of nucleon strings in the central region of the model may cause different deformations.

References

[1] Mayer M G & Jensen J H D 1955 Elementary theory of nuclear shell structure *Nuclear Physics* 1(9): 670-671.
[2] Bohr A & Mottelson B 1969 *Nuclear Structure, Vol. 1. Single-Particle Motion* (worldscientific, New York Heidelberg Berlin).
[3] Rydin R A 2011 New magic numbers in the continent of isotopes. *Annals of Nuclear Energy* **38**, 2356–2358.
[4] Sorlin O & Porquet M-G 2008 Nuclear magic numbers: New features far from stability. *Progress in Particle and Nuclear Physics* **61** 602–673.
[5] Hagen G, Hjorth-Jensen M, Jansen G R, Machleidt R & Papenbrock T 2012 Evolution of shell structure in neutron-rich calcium isotopes *Phys. Rev. Lett.* **109** 032502.
[6] Otsuka T, Gade A, Sorlin O, Suzuki T & Utsuno Y 2020 Evolution of shell structure in exotic nuclei. *Rev. Mod. Phys.* **92** 015002.
[7] Angeli I & Marinova K 2013 Table of experimental nuclear ground state charge radii: An update. *Atomic Data and Nuclear Data Tables* **99** 69–95.
[8] Stodolna A S et al. 2013 Hydrogen atoms under magnification: Direct observation of the nodal

structure of stark states. *Phys. Rev. Lett.* **110** 213001.
[9] Hen O, Miller G A, Piasetzky E & Weinstein L B 2017 Nucleon-nucleon correlations, short-lived excitations, and the quarks within. *Rev. Mod. Phys.* **89** 045002.
[10] Maxwell J C 2011 *The Scientific Papers of James Clerk Maxwell I*. Cambridge Library Collection - Physical Sciences (Cambridge University Press).
[11] Irvine W T M & Bouwmeester D 2008 Linked and knotted beams of light. *Nature Physics* **4** 716–720.
[12] Thomson W 1867 On vortex atoms. *The London, Edinburgh, and Dublin Philosophical Magazine and Journal of Science* **34** 15–24.
[13] Faddeev L & Niemi A J 1997 Stable knot-like structures in classical field theory. *Nature Physics* **387** 58–61.
[14] Dennis M R, King R P, Jack B, O'Holleran K & Padgett M J 2010 Isolated optical vortex knots. *Nature Physics* **6** 118–121.
[15] Hall D S et al. 2016 Tying quantum knots *Nature Physics* **12** 478–483.
[16] Kedia H, Bialynicki-Birula I, Peralta-Salas D et al. 2013 Tying knots in light fields. *Phys. Rev. Lett.* **111** 150404.
[17] Veneziano G 1968 Construction of a crossing-simmetric, regge-behaved amplitude for linearly rising trajectories. *Il Nuovo Cimento A (1965-1970)* **57** 190–197.
[18] Nambu Y 1970 Quark model and the factorization of the Veneziano amplitude *Proc. Int. Conf. on Symmetries and Quark Models* 258–267.
[19] Kaku M 1988 *Nambu-Goto Strings* P7 (Springer US, New York, NY).
[20] Nielsen H & Olesen P 1973 Vortex-line models for dual strings. *Nuclear Physics B* **61** 45–61.
[21] Nielsen H B 2009 String from veneziano model. *arXiv: High Energy Physics - Phenomenology*.
[22] Susskind L 1969 Harmonic-oscillator analogy for the veneziano model *Phys. Rev. Lett*. **23** 545–547.
[23] Coursey J S, Schwab D J, Tsai J J & Dragoset R A 2015 *Atomic weights and isotopic compositions (version 4.1)* (National Institute of Standards and Technology, Gaithersburg, MD).
[24] Johnson R C & Oi M 2010 Nuclear superfluidity. pairing in finite systems, by d.m. brink and r.a. broglia *Contemporary Physics* **51** 91–92.
[25] Johnson C W, Bertsch G F & Dean D J 1998 Orderly spectra from random interactions *Phys. Rev. Lett.* **80** 2749–2753.
[26] Rowe D J & Goldhammer P 2010 *Nuclear collective motion: Models and theory*.
[27] Cederwall B, Moradi F G, Bäck T et al. 2011 vidence for a spin-aligned neutron–proton paired phase from the level structure of 92pd. *Nature* **469** 68–71.
[28] Gell-Mann M 1964 A schematic model of baryons and mesons *Physics Letters* **24** 923–925.
[29] Bloom, E. D. et al. 1969 High-energy inelastic e − p scattering at 6° and 10°. *Phys. Rev. Lett.* **23**, 930–934.
[30] Breidenbach, M. et al. 1969 Observed behavior of highly inelastic electron-proton scattering. *Phys. Rev. Lett.* **23**, 935–939.
[31] Gross D J 2005 Nobel lecture: The discovery of asymptotic freedom and the emergence of qcd *Rev. Mod. Phys.* **77** 837–849.
[32] Thakur V et al. 2020 Microscopic study of the shell structure evolution in isotopes of light to middle mass range nuclides *Nuclear Physics A* **1002** 121981.
[33] Kanungo R, Tanihata I & Ozawa A 2002 Observation of new neutron and proton magic numbers *Physics Letters B* **528** 58–64.
[34] Cortina-Gil D, Fernandez-Vazquez J, Aumann T et al. 2004 Shell structure of the near-dripline nucleus 23O *Phys. Rev. Lett.* **93** 062501.
[35] Fridmann J, Wiedenhöver I, Gade A et al. 2005 'magic' nucleus 42Si. *Nature* **435** 922–924.
[36] Sargsian M M, Weinstein L B, Piasetzky E et al. 2016 *The cafe experiment: Short-range pairing mechanisms in heavy nuclei proposal to jefferson lab pac* **44.**

[37] Johnson C W, Bertsch G F & Dean D J 1998 Orderly spectra from random interactions *Phys. Rev. Lett.* **80** 2749–2753.
[38] Freer M 2007 The clustered nucleus—cluster structures in stable and unstable nuclei *Reports on Progress in Physics* **70** 2149.
[39] Duer M, Aumann T et al. 2022 Observation of a correlated free four-neutron system *Nature* **606** 678–682.
[40] Talmi I 1993 *Simple Models of Complex Nuclei (1st ed.)*, vol. 1 (Routledge).
[41] Committee T D N S A 2008 *The frontiers of nuclear science, a long range plan*.
[42] Rutherford H 1920 Nuclear constitution of atoms *Proc. Roy. Soc. A* **97** 374.
[43] Wood J 2013 Simple structure in complex nuclei *Physics* **6** 52.
[44] Yordanov D T et al. 2013 Spins, electromagnetic moments, and isomers of 107−129Cd *Phys. Rev. Lett.* **110** 192501.
[45] Cheng Y Y et al. 2019 Nucleon-pair picture of low-lying states in semi-magic and open-shell nuclei *Phys. Rev. C* **100** 024321.
[46] Ruiz R F G & Vernon A R 2020 Emergence of simple patterns in many-body cs: from macroscopic objects to the atomic nucleus *The European Physical Journal A* **56** 136.
[47] Wong C Y 2019 Toroidal states of the 12c nucleus *Bulgarian Journal of Physics* **46**.
[48] Cao, X. G. et al. α and α Conjugate Fragment Decay from the Disassembly of ^{28}Si at Very High Excitation Energy (JPS, 2020).
[49] Winter M 2021 *A gallery of orbitals on the orbitron*.
[50] Werner S A, Colella R, Overhauser A W et al. 1975 Observation of the phase shift of a neutron due to precession in a magnetic field *Phys. Rev. Lett.* **35** 1053–1055.
[51] Ichikawa T, Matsuyanagi K, Maruhn J A & Itagaki N 2014 Pure collective precession motion of a high-spin torus isomer *Phys. Rev. C* **89** 011305.
[52] Pastore S 2016 Electromagnetic structure of light nuclei *EPJ Web of Conferences* **113** 01008.
[53] Ablikim M, Achasov M N, Adlarson P et al. 2021 Oscillating features in the electromagnetic structure of the neutron. *Nature Physics* **17** 1200–1204.
[54] Michel, N. & Płoszajczak, M. 2021 Gamow Shell Model (*Springer Cham*).
[55] de Groote, R. P. & Neyens, G. 2020 Spins and Electromagnetic Moments of Nuclei, 15–17 (*Springer Nature Singapore*).
[56] Olive, K. 2014 Review of particle physics. *Chinese Physics C* **38**, 090001.
[57] Feynman R 1963 *The Feynman Lectures on Physics Vol. 1*, chap. **52** 16–17 (Addison-Wesley,).
[58] Frauenfelder H, Bobone R, von Goeler E et al. 1957 Parity and the polarization of electrons from co60 *Phys. Rev.* **106** 386–387.
[59] Ford, K. W. John Wheeler's work on particles, nuclei, and weapons. *Physics Today* **62**, 29–33 (2009).
[60] Klein O 1929 Die reflexion von elektronen an einem potentialsprung nach der relativistischen dynamik von dirac *Zeitschrift für Physik* **53** 157–165.
[61] Alvarez L W 1969 Recent developments in particle physics *Science* **165** 1071–1091.
[62] Park H, Cai J, Anderson E et al. 2023 Observation of fractionally quantized anomalous hall effect *Nature* **622** 74–79.
[63] Lu Z, Han T, Yao Y et al. 2024 Fractional quantum anomalous hall effect in multilayer graphene *Nature* **626** 759–764.